AEROELASTIC ANALYSIS OF HELICOPTER ROTOR BLADES INCORPORATING ANISOTROPIC PIEZOELECTRIC TWIST ACTUATION

W. Keats Wilkie
NASA Langley Research Center
Aeroelasticity Branch
Mail Stop 340
Hampton, Virginia 23681-0001, U.S.A.
phone: (757) 864-1260, fax: (757) 864-8678
e-mail: w.k.wilkie@larc.nasa.gov

W. Keith Belvin
NASA Langley Research Center
Structural Dynamics Branch
Mail Stop 230
Hampton, Virginia 23681-0001, U.S.A.
phone: (757) 864-4319, fax: (757) 864-8540
e-mail: w.k.belvin@larc.nasa.gov

K. C. Park
University of Colorado at Boulder
Center for Aerospace Structures
Campus Box 429
Boulder, Colorado 80309-0429, U.S.A.
phone: (303) 492-6330, fax: (303) 492-4990
e-mail: kcpark@titan.colorado.edu

ABSTRACT

A simple aeroelastic analysis of a helicopter rotor blade incorporating embedded piezoelectric fiber composite, interdigitated electrode blade twist actuators is described. The analysis consists of a linear torsion and flapwise bending model coupled with a nonlinear ONERA based unsteady aerodynamics model. A modified Galerkin procedure is performed upon the rotor blade partial differential equations of motion to develop a system of ordinary differential equations suitable for dynamics simulation using numerical integration. The twist actuation responses for three conceptual full-scale blade designs with realistic constraints on blade mass are numerically evaluated using the analysis. Numerical results indicate that useful amplitudes of nonresonant elastic twist, on the order of one to two degrees, are achievable under one-g hovering flight conditions for interdigitated electrode poling configurations. Twist actuation for the interdigitated electrode blades is also compared with the twist actuation of a conventionally poled piezoelectric fiber composite blade. Elastic twist produced using the interdigitated electrode actuators was found to be four to five times larger than that obtained with the conventionally poled actuators.

NOMENCLATURE

A	rotor disk area, πR^2; spar material cross sectional area, m^2
A_e	thin-walled spar section enclosed area, m^2
a	lift curve slope, rad^{-1}
b	blade semichord, $c/2$, m
$\bar{b}$	normalized blade semichord, b/R
C_m	airfoil pitching moment coefficient, $C_m=M_\theta/(1/2)\rho V^2c^2$
C_{ml}	linear model static pitching moment coefficient
C_{ms}	measured static pitching moment coefficient
C_T	rotor thrust coefficient, $C_T=T/\rho A\Omega^2R^2$
C_z	airfoil lift coefficient, $C_z=L/(1/2)\rho V^2c$
C_{zl}	linear model static lift coefficient
C_{zs}	measured static lift coefficient
c	blade chord, m; section contour length, m
$\bar{c}$	normalized blade chord, c/R
c_1, c_2, c_3	pitching moment coefficients
c_{ij}	material stiffnesses, N/m^2
D_i	electrical displacements, $Coulombs/m^2$
d_{ij}	piezoelectric strain constants, Coulombs/N or m/V
$EI_{\eta\eta}$	effective bending stiffness of composite blade structure, $\oint K_{11}z^2ds$, $N\text{-}m^2$
E_i	electric field intensities, V/m
E^*	coefficient of internal friction in tension, $N/m^2/sec$
e	distance of section mass center forward of pitch axis, m
$\bar{e}$	normalized distance of section mass center forward of pitch axis, e/R
e_{ij}	piezoelectric stress constants, $Coulomb/m^2$
f	equivalent flat plate drag area of fuselage, m^2
GJ	effective torsional stiffness of composite blade structure, $\frac{4A_e^2}{c^2}\oint K_{22}ds$, $N\text{-}m^2$
G^*	coefficient of internal friction in shear, $N/m^2/sec$
h	height of rectangular spar cross-section, m
I_β	blade flapping inertia, $\int_0^R mr^2dr$, $kg\text{-}m^2$
I_θ	blade pitch mass moment of inertia, $\int_0^R mk_m^2dx$, $kg\text{-}m^2$
K_{ij}	effective laminate stiffnesses neglecting hoop stress, N/m
K_β	blade flapping root spring rate, N-m/rad
K_θ	blade pitch root spring rate, N-m/rad
k_A	polar radius of gyration of cross-section area about the elastic axis, m

k_m polar radius of gyration of cross-section mass about the elastic axis, $k_m^2=k_{m1}^2+k_{m2}^2$, m

k_{m1} mass radius of gyration about section y_3 axis, m

k_{m2} mass radius of gyration about section z_3 axis, m

$\bar{k}$ average value of inverse of reduced velocity, b/x

L airfoil section aerodynamic lift per unit length, N/m

L_z aerodynamic force per unit length in z_0 direction, N/m

$\bar{L}_w$ nondimensional aerodynamic force per unit length in z_0 direction, $L_w/m\Omega^2R$

M section Mach number

M_{PE} induced piezoelectric bending moment, N-m

M_ϕ, M_θ aerodynamic pitching moment per unit length about $c/4$, N-m/m

$\bar{M}_\phi$ nondimensional aerodynamic pitching moment, $M_\phi/m\Omega^2R^2$

m blade mass per unit length, kg/m

N number of aerodynamic evaluation points along blade

Q number of rotor blades

Q_{PE} piezoelectric induced twisting moment, N-m

r distance perpendicular from section contour tangent to origin, m

R rotor radius, m

S_i material strains, m/m

s_{ij} material compliances, m^2/N

T rotor thrust, N;
blade tension force, N

T_i material stresses, N/m^2

t time, sec;
spar wall total thickness, m

t_{PE} total thickness of piezoelectric material, m

U airfoil section normalized velocity, $V/\Omega R$

u blade axial elastic deflection, m

$\bar{u}$ normalized blade axial deflection, $\bar{u} \equiv u/R$

V airfoil section velocity, m/sec

V_∞ helicopter forward flight velocity, m/sec

W bending modal function

w out-of-plane elastic deflection, m;
width of rectangular spar cross-section, m

$\bar{w}$ normalized blade out-of-plane elastic deflection, $\bar{w} \equiv w/R$

x blade radial coordinate, m

$\bar{x}$ nondimensional radial coordinate, x/R

$\bar{x}_i$ normalized midpoint position of ith aerodynamic segment

$x_3y_3z_3$ reference system fixed in deformed blade, with x_3 axis tangent to the deformed blade elastic axis

y_{ac} distance of aerodynamic center forward of pitch axis, m

$\bar{y}_{ac}$ normalized distance of aerodynamic center forward of pitch axis, y_{ac}/c

α airfoil section angle of attack, rad

α_s rotor shaft angle, rad

Δ_i normalized width of ith aerodynamic segment

ε_{ij} permittivities of piezoelectric material, Farad/m

$\mathcal{E}^*$ section rotation rate with respect to the air mass

Φ torsion modal function

ϕ torsional deflection, rad

γ blade Lock number, $\gamma=\rho acR^4/I_\beta$

$\bar{\Gamma}$ section nondimensional circulation, $\bar{\Gamma} = \bar{L}_z/U$

$\bar{\Gamma}_1$ linear model (unstalled) component of section nondimensional circulation

$\bar{\Gamma}_2$ component of section nondimensional circulation due to stall

$\bar{\Gamma}_{m2}$ normalized section pitching moment deviation due to stall

μ rotor advance ratio, $V_\infty/\Omega R$

θ section pitch angle, $\theta=\theta_{con}+\phi$, rad

θ_0 blade collective pitch input angle, rad

θ_{1c} longitudinal cyclic pitch input, rad

θ_{1s} lateral cyclic pitch input, rad

θ_{con} blade control pitch setting, $\theta_{con}=\theta_0+\theta_{1c}cos\psi+\theta_{1s}sin\psi$, rad

θ_{ply} piezoelectric material ply rotation angle, rad

ρ air density, kg/m^3

σ rotor solidity, $\sigma=Qc/\pi R$

Ω rotor rotational speed, rad/sec

$\bar{\omega}_\phi$ nondimensional root pitch natural frequency, $\sqrt{K_\phi/I_\theta\Omega^2}$

ψ nondimensional time (blade azimuth angle), $\psi=\Omega t$, rad

$(\,)^E$ constant electric field value

$(\,)^S$ constant strain value

$(\,)^T$ constant stress value

$(\,)^t$ matrix transpose

$\sim$
$(\,)$ rotated system value

$\overset{*}{(\,)}$ $d(\,)/d\psi$

$(\,)^+$ $d(\,)/d\bar{x}$

1. INTRODUCTION

High vibratory loads problems exist throughout today's civil and military helicopter fleet. Such vibratory loads place severe limits on the reliability and maintainability of vibration sensitive helicopter hardware, as well as limit the load carrying and forward flight speed capabilities of these vehicles. As a result, a high priority has been placed on reducing or eliminating these vibratory loads, and much work has been performed to develop various passive and active methods and mechanisms for achieving this task (Reichert, 1981; Loewy, 1984).

The primary sources of rotorcraft vibration can be traced to effects associated with the unsteady aerodynamic environment of the main rotor system. High tip Mach numbers on the advancing blade side, and stall effects on the retreating blade side produce many of the high oscillatory forces experienced by the rotor blades. Blade-vortex interaction and fuselage interference effects are also additional aerodynamic sources of rotor vibrations.

Past conventional rotorcraft vibration reduction schemes have often focused on dampening or alleviating undesirable vibrations after the fact. More recent active control techniques seek to eliminate or reduce these vibrations at their source, namely by modifying the unsteady aerodynamic forces acting upon individual rotor blades. These are the so-called "individual blade control" techniques, or IBC

(Ham, 1987). Some form of IBC will most likely be required for future helicopters if the goal of a "jet smooth" ride is ever to be met.

1.1 Smart material IBC actuation schemes.

Although the IBC concept itself is not new, providing a practical means of actuating on-blade control surfaces, pitch, or twist of individual blades remains the principal difficulty in implementing individual blade control techniques on actual helicopters. Adaptive, or smart, materials have been examined by many researchers as a means of providing these sorts of actuation without employing complicated electromechanical or hydraulic mechanisms.

Flap actuation techniques using adaptive materials can, in principal, provide the power and displacement necessary to be used as a means of vibration suppression, and the development of effective smart material flap actuators has been examined by many researchers (Spangler and Hall, 1990; Samak and Chopra, 1993; Giurgiutiu, et al, 1995). This approach still requires placement of additional mechanisms, with an attendant increase in complexity, into the rotating system. The requirement that much of the mass of these mechanisms must be placed aft of the blade pitch axis is also an undesirable characteristic. A more desirable technique, in terms of mechanical simplicity and aerodynamic efficiency, is the production of active blade twist through piezoelectric material actuators embedded in the blade structure (Barrett, 1990; Chen and Chopra, 1993; Derham and Hagood, 1996). Unfortunately, the effectiveness of the majority of these smart material twist actuation schemes, to date, has been relatively poor due, primarily, to the limited power and displacement capabilities of the available smart materials.

Despite these drawbacks, some encouraging developments in twist actuation of smart material structures continue to be made. Most recently, research in anisotropic twist actuation of plate structures using piezoelectric fiber composites (PFC) (Rodgers and Hagood, 1995; Bent, et al, 1995) has demonstrated that relatively high levels of twist actuation are potentially achievable. The application of interdigitated electrode technology (IDE) (Hagood, et al, 1993; Bent and Hagood, 1995) can in principle enhance the performance of these materials even further.

1.2 Previous work related to analysis of embedded smart material actuated rotor structures.

To date, there has been relatively little analytical work reported detailing the aeroelastic behavior of rotor blades incorporating embedded smart material actuators. Song and Lebrescu (1993) developed the equations of motion for a rotating, thin-walled, cantilevered beam structure incorporating embedded piezoelectric actuators. No aerodynamics were included in their study, and actuation of torsional motion was not considered. Nitzsche and Breitbach (1994) reported results of an analytical study to evaluate the ability of embedded piezoelectric materials to attenuate out-of-plane bending and torsional vibrations on a rotor blade structure. To accomplish this, they developed a rotor blade aeroelastic model incorporating quasi-static aerodynamics and a "directionally attached piezoelectric crystal" bending-torsion actuation scheme similar to that developed by Barrett. They concluded that the lightly damped torsional blade modes could be significantly affected on a practical blade structure without saturation of the piezoelectric materials.

Most recently, Derham and Hagood (1996) described work related to a joint Boeing/MIT effort to develop a system for actively twisting helicopter blades using interdigitated electrode piezoelectric fiber composite plies. They report achieving levels of twist up to 1.4 degrees in a bench test of a 1/16 Froude scaled model rotor blade. The vibration reduction potential of a proposed 1/6 Mach scaled model blade was also examined using a modified version of Boeing's TECH-01 comprehensive rotor analysis program. This analysis indicated that 70% to near 100% reductions in the 3Ω vertical hub shears (the principal vibratory load) could be achieved using an appropriately phased 3Ω frequency applied twisting moment couple. A couple magnitude associated with the maximum theoretically produceable level of piezoelectric strain was used in this study.

1.3 Scope of this effort.

For the most part, aeroelastic analysis of rotor blades incorporating embedded smart material strain actuation is still very much in its infancy. In particular, there is a lack of simple analytical models suitable for conducting preliminary conceptual control and design studies for such rotor blade structures. In light of this, and in order to gain greater insight into the control and aeroelastic response issues related to induced twist smart structure rotor blades, a simple aeroelasticity model for a piezoelectric twist actuated helicopter rotor blade has been developed by the authors. This model is derived specifically for use in the investigation of phenomena related to torsional control and response of helicopter rotor blades incorporating piezoelectric twist. Terms related to both stiffness and piezoelectric free strain anisotropy have been included, which allows for a wide variety of piezoelectric actuation concepts to be evaluated. In this paper, a description of the derivation and numerical implementation of this model is given. Additionally, numerical examples demonstrating the twist actuation potential of three conceptual full-scale helicopter blade designs, each employing a representative form of piezoelectric actuation, are shown.

2. ANALYTICAL MODEL DESCRIPTION

In this section we will present aeroelastic equations of motion for a piezoelectric actuated helicopter rotor blade. For simplicity, only linear out-of-plane bending and torsion structural dynamics will be considered here. The aerodynamic formulation will follow a finite-state strip-theory approach, but will include a dynamic stall representation based on the ONERA model. The blade structural geometry will be idealized as a rectangular, closed-cell, thin-walled composite beam containing embedded piezoelectric material layers (Fig. 1), and we will develop the piezoelectric actuation equations for this structure allowing for stiffness and piezoelectric free strain anisotropy within the piezoelectric laminae.

2.1 Structural formulation

The equations of motion used here to were adapted from the general elastic bending and torsion deformation equations developed by Kaza and Kvaternik (1977). Due to the complexity of these equations, and elastic rotor blade equations of motion in general, it was necessary to apply some simplifying assumptions to the complete set of equations in order to obtain a more mathematically manageable model. An ordering scheme approach was used here to accomplish this. Use of such a procedure ensures that the most physically significant terms are retained, while allowing small terms to be consistently neglected. The ordering of parameters used in this study

was based on schemes applicable to rotorcraft vibrations, and is given in Wilkie and Park (1996).

Additional assumptions made to simplify the equations were, 1) that the blade precone angle and built in twist were assumed to be zero, 2) the blade structural cross-section was assumed to be doubly symmetric, and 3) the blade pitch radius of gyration could be approximated by the k_{m2} cross section integral (i.e., $k_{m1}/k_{m2}<<1$). Small angles were assumed throughout for θ_{con} and ϕ.

Applying the ordering scheme, with the additional assumptions listed above, to Kaza and Kvaternik's equations yields the following nondimensional partial differential equations of motion for blade out-of-plane bending and torsion.

Out-of-plane (flapwise) bending:

$$\begin{aligned}&\overline{\overline{w}}-\left(\frac{T}{m\Omega^2R^2}\overline{w}^{+}\right)^{+}+\bar{e}\left(\overline{\overline{\phi}}+\overline{\overline{\theta}}_{con}\right)-\left\{\bar{e}\bar{x}\left(\theta_{con}+\phi\right)\right\}^{+}\\&+\left\{\frac{EI_{\eta\eta}}{m\Omega^2R^4}\overline{w}^{++}\right\}^{++}+\left\{\frac{E^{*}I_{\eta\eta}}{m\Omega R^4}\overline{\overline{w}}^{*++}\right\}^{++}=\frac{L_w}{m\Omega^2R}+\left(\frac{M_{PE}}{m\Omega^2R^3}\right)^{++}\end{aligned}\tag{1}$$

Torsional deformation:

$$\begin{aligned}&\frac{k_m^{\,2}}{R^2}\left(\overline{\overline{\phi}}+\overline{\overline{\theta}}_{con}\right)+\frac{k_m^{\,2}}{R^2}\phi-\left[\frac{T}{m\Omega^2R^2}\frac{k_A^{\,2}}{R^2}\phi^{+}\right]^{+}\\&+\bar{e}\left[\bar{x}\overline{w}^{+}+\overline{\overline{w}}\right]-\left(\frac{GJ}{m\Omega^2R^4}\phi^{+}\right)^{+}-\left(\frac{G^{*}J}{m\Omega R^4}\overline{\phi}^{*+}\right)^{+}\\&=\frac{M_\phi}{m\Omega^2R^2}-\left(\frac{Q_{PE}}{m\Omega^2R^3}\right)^{+}-\frac{k_m^{\,2}}{R^2}\theta_{con}\end{aligned}\tag{2}$$

The blade section tension force, T, is approximately given by

$$T\cong\Omega^2R^2\int_{\bar{x}}^{1}m\bar{x}d\bar{x}\tag{3}$$

Rotor blade coordinate systems and deflections are shown in Fig. 2. M_{PE} and Q_{PE} in Eq. (1) and Eq. (2) are the additional terms representing the piezoelectric induced bending and twisting moments produceable with the blade structure. These terms will be derived in the piezoelectric control moment section below.

A modified Galerkin procedure (Duncan, 1937) is used here to obtain modal solutions to Eqs. (1)-(3). In this case, superposition solutions for w and ϕ of the form,

$$\overline{w}(\bar{x},\psi)=\sum_{l=1}^{L}\overline{w}_l(\psi)W_l(\bar{x})\tag{4}$$

$$\phi(\bar{x},\psi)=\sum_{m=1}^{M}\phi_m(\psi)\Phi_m(\bar{x})\tag{5}$$

are assumed, where L and M are the number of out-of-plane bending and torsional modal functions respectively. In the modified Galerkin procedure, these modal functions need only satisfy the geometric boundary conditions on the blade. Work due to any nonfulfilled natural boundary conditions is accounted for with additional boundary terms in the equations. Substituting Eqs. (4)-(5) into Eq. (1), and performing the appropriate integrations, yields a set of L ordinary differential equations of the following form:

$$\begin{aligned}&\sum_{l=1}^{L}\overline{\overline{w}}_l\int_0^1W_lW_nd\bar{x}+\sum_{l=1}^{L}\overline{\overline{w}}_l\int_0^1\frac{E^{*}I_{\eta\eta}}{m\Omega R^4}W_l^{++}W_n^{++}d\bar{x}\\&+\sum_{l=1}^{L}\overline{w}_l\Big(\int_0^1\frac{T}{m\Omega^2R^2}W_l^{+}W_n^{+}d\bar{x}+\int_0^1\frac{EI_{\eta\eta}}{m\Omega^2R^4}W_l^{++}W_n^{++}d\bar{x}\\&+\frac{K_\beta}{\Omega^2R^3\int_0^1md\bar{x}}W_l^{+}(0)W_n^{+}(0)\Big)\\&+\sum_{m=1}^{M}\overline{\overline{\phi}}_m\int_0^1\bar{e}\Phi_mW_nd\bar{x}+\sum_{m=1}^{M}\phi_m\int_0^1\bar{e}\bar{x}\Phi_mW_n^{+}d\bar{x}\\&=\int_0^1\frac{L_w}{m\Omega^2R}W_nd\bar{x}+\int_0^1\frac{M_{PE}}{m\Omega^2R^3}W_n^{++}d\bar{x}\\&-\left(\overline{\overline{\theta}}_{con}\int_0^1\bar{e}W_nd\bar{x}+\theta_{con}\int_0^1\bar{e}\bar{x}W_n^{+}d\bar{x}\right)\end{aligned}\tag{6}$$

where $n=1,L$. A similar procedure performed on Eq. (2) yields an additional set of M ordinary differential equations;

$$\begin{aligned}&\sum_{m=1}^{M}\overline{\overline{\phi}}_m\int_0^1\frac{k_m^{\,2}}{R^2}\Phi_m\Phi_pd\bar{x}+\sum_{m=1}^{M}\overline{\phi}_m\int_0^1\frac{G^{*}J}{m\Omega R^4}\Phi_m^{+}\Phi_p^{+}d\bar{x}\\&+\sum_{m=1}^{M}\phi_m\Big(\int_0^1\frac{k_m^{\,2}}{R^2}\Phi_m\Phi_pd\bar{x}+\int_0^1\frac{T}{m\Omega^2R^2}\frac{k_A^{\,2}}{R^2}\Phi_m^{+}\Phi_p^{+}d\bar{x}\\&+\int_0^1\frac{GJ}{m\Omega^2R^4}\Phi_m^{+}\Phi_p^{+}d\bar{x}+\frac{K_\theta}{\Omega^2R^3\int_0^1md\bar{x}}\Phi_m(0)\Phi_p(0)\Big)\\&+\sum_{l=1}^{L}\overline{\overline{w}}_l\int_0^1\bar{e}W_l\Phi_pd\bar{x}+\sum_{l=1}^{L}\overline{w}_l\int_0^1\bar{e}\bar{x}W_l^{+}\Phi_pd\bar{x}\\&=\int_0^1\frac{M_\phi}{m\Omega^2R^2}\Phi_pd\bar{x}+\int_0^1\frac{Q_{PE}}{m\Omega^2R^3}\Phi_p^{+}d\bar{x}\\&-\left(\overline{\overline{\theta}}_{con}+\theta_{con}\right)\int_0^1\frac{k_m^{\,2}}{R^2}\Phi_pdx\end{aligned}\tag{7}$$

with $p=1, M$.

The K_β and K_θ terms in Eqs. (6)-(7), which do not appear in Eqs. (3)-(4), are used to represent finite stiffnesses present at $\bar{x}=0$. These terms can be used to account for the stiffness of a mechanical flapping spring placed at the blade root, or the inherent flexibility of the pitch control system.

Stiffness terms (GJ, $EI_{\eta\eta}$) in the above equations represent the effective stiffnesses of the combined piezoelectric/passive material blade structure. These terms were derived using the thin-walled, closed section, composite beam theory developed by Rehfield (1985). We have assumed that the resulting composite structure is elastically uncoupled, hence, potential elastic coupling terms have been ignored. The detailed derivation of the stiffness terms is given in Wilkie and Park (1996).

2.2 Aerodynamic formulation

The sectional lifting forces and moments are calculated using a technique based on the ONERA dynamic stall model developed by Tran and Petot (1981). The ONERA model uses differential equations in time to describe the unsteady aerodynamic lifting forces and pitching moments, including dynamic stall effects, acting upon an airfoil section undergoing arbitrary pitch and plunge motion.

2.2.1 Section lift formulation

Modifications to the ONERA model for general use in rotorcraft aerodynamic formulations have been made by Peters (1985), with nondimensional circulations employed as state variables instead of aerodynamic coefficients. The simplified lift circulation equations reported therein, which are well behaved in the reverse flow region of the rotor disk but do not give lift reversal, are used here (Eqs. (8)-(12)).

$$\bar{L}_Y = \bar{L}_0 + U_X\left(\bar{\Gamma}_1 + \bar{\Gamma}_2\right) \tag{8}$$

$$\bar{L}_X = -U_Y\left(\bar{\Gamma}_1 + \bar{\Gamma}_2\right) \tag{9}$$

$$\bar{L}_0 = \bar{b}\, s_z \overset{*}{U}_Y \tag{10}$$

$$\bar{k}\overset{*}{\bar{\Gamma}}_1 + \lambda_z\bar{\Gamma} = \lambda_z a U_Y + \delta_z \bar{b}\overset{*}{\varepsilon} \tag{11}$$

$$\begin{aligned}\bar{k}^2\overset{**}{\bar{\Gamma}}_2 + 2d_z w_z \bar{k}\overset{*}{\bar{\Gamma}}_2 + w_z^2\left(1+d_z^2\right)\bar{\Gamma}_2 \\ = -w_z^2\left(1+d_z^2\right)\left[U_X\Delta C_z + e_z\bar{k}\left(\overset{*}{U}_X\Delta C_z + \frac{\partial \Delta C_z}{\partial\alpha}\overset{*}{U}_Y\right)\right]\end{aligned} \tag{12}$$

$\bar{L}_0$ in Eq. (10) is the nondimensional apparent mass lift. $\bar{L}_X$ and $\bar{L}_Y$ are the components of the nondimensional lift in the airfoil section X and Y directions respectively, and $\overset{*}{\varepsilon}$ is the geometric rate of rotation of the airfoil with respect to the air mass. The nondimensional section velocities U, U_X and U_Y and section angle of attack, α, used in this study are presented in detail in Wilkie and Park (1996).

ΔC_z in Eq.(12) is the difference between the linear model static lift coefficient, C_{zl} and the measured stalled lift coefficient, C_{zs}, i.e., $\Delta C_z = C_{zl} - C_{zs}$,. The angle of attack dependent coefficients (s, λ, δ, d, w, and e) are derived from experimental two-dimensional unsteady airfoil tests using the parameter identification scheme described in

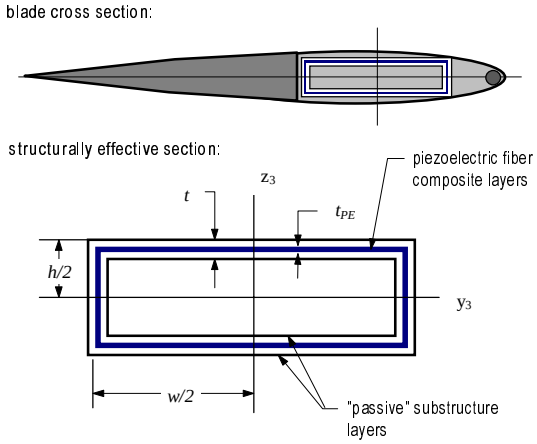

Figure 1. Idealized rectangular, thin-walled, closed-section piezoelectric blade structure.

Tran and Petot (1981). ONERA OA212 airfoil static lift coefficient data and stall parameter values were used in this model (Peters, et al, 1990).

2.2.2 Section Pitching Moment Formulation

Improvements to the basic ONERA pitching moment formulation have been made by Petot (1989) with further modifications made by Peters, et al (1990), and this is the representation used in this model. In this approach, the unstalled component of C_m is given explicitly through the static moment coefficient, which is a function of angle-of-attack only. This results in the elimination of one state per spanwise aerodynamic evaluation point in the model. Static pitching moment data used here was extrapolated from curves given in Peters, et al (1990), and from data provided by Tang (1995).

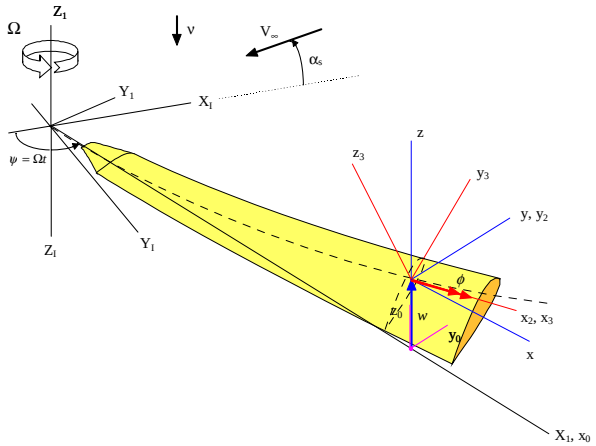

Figure 2. Rotor blade coordinate systems and deflections.

The stalled contribution to the section pitching moment is calculated using a circulation based model similar to that developed for section lift. The second order differential equation describing this stalled pitching moment circulation, defined as $\bar{\Gamma}_{m2} \equiv UC_{m2}$, is shown below (13).

$$\bar{k}_i^{\,2}\overset{**}{\bar{\Gamma}}_{m2i} + a_{mi}\bar{k}_i\overset{*}{\bar{\Gamma}}_{m2i} + r_{mi}\bar{\Gamma}_{m2i} = -r_{mi}U_i\Delta C_{mi} - E_{mi}\bar{k}_i\overset{*}{\bar{U}}_{y_i} \tag{13}$$

The coefficients a_m, r_m, and E_m in Eq. (13) were found by Petot (1989) to have similar characteristics for many airfoils. Expressions for these coefficients, omitting subscripts, may be written as

$$a_m = a_0 + a_2\Delta C_z^{\,2} \tag{14}$$

$$r_m = \left(r_0 + r_2\Delta C_z^{\,2}\right)^2 \tag{15}$$

$$E_m = E_2\Delta C_z^{\,2} \tag{16}$$

Values of a_0, a_2, r_0, r_2, and E_2 used in the present formulation are taken from the generic "mean airfoil" values proposed by Petot (1989).

2.2.3 Airloads calculation

The aerodynamic forcing integrals present in Eqs. (6)-(7) were calculated by evaluating the sectional aerodynamic forces and moments per unit length at N discrete points along the blade span. For ease of integration, section aerodynamic forces and moments were assumed to be constant over the width of each section. Consistent with the ordering scheme assumed in the structural formulation above, the final expressions for these aerodynamic loading integrals are

$$\int_0^1 \bar{L}_w W_l d\bar{x} \cong \frac{\gamma}{6a}\sum_{i=1}^{N}\left\{U_i\left(\bar{\Gamma}_{1_i} + \bar{\Gamma}_{2_i}\right) + \bar{L}_{0_i}\right\}\int_{\bar{r}_i}^{\bar{r}_{i+1}} W_l d\bar{x} \tag{17}$$

$$\int_0^1 \bar{M}_\phi \Phi_m d\bar{x} = \frac{\gamma\bar{c}}{6a}\sum_{i=1}^{N}\left\{U_i^{\,2}C_{m\ell i} + U_i\bar{\Gamma}_{m2i} + c_1\bar{b}\,\overset{*}{\bar{U}}_{y_i} + c_2U_i\overset{*}{\varepsilon}\Big|_{\bar{x}_i} + c_3\bar{b}^{\,2}\left(\overset{**}{\theta}_{con} + \overset{**}{\phi}\right)\Big|_{\bar{x}_i} + \bar{y}_{ac}\left[U_i\left(\bar{\Gamma}_{1_i} + \bar{\Gamma}_{2_i}\right) + \bar{L}_{0_i}\right]\right\}\int_{\bar{r}_i}^{\bar{r}_{i+1}} \Phi_m d\bar{x} \tag{18}$$

(Note that the lifting moment expression used here (17), is an approximation valid for small θ and conditions where $U_Y << U_X$.)

$\bar{r}_i$, in Eqs. (17)-(18), is the radial location of the inboard edge of the ith aerodynamic section, $\bar{r}_i = \bar{x}_i - \Delta_i/2$, where $\bar{x}_i$ is the nondimensional radial location of the ith aerodynamic evaluation point, and Δ_i the associated nondimensional section width.

A uniform rotor inflow model, based on momentum theory (Gessow and Myers, 1952), was used for this formulation. This assumption of constant inflow velocity at every location across the rotor disk is adequate for modelling hovering or vertical flight conditions, but not realistic for forward flight. Nevertheless, it is used here for computational simplicity in the numerical model. More complex inflow representations will be incorporated into future versions of this analysis.

Swashplate control angles (θ_0, θ_{1c} θ_{1s}) required for trim were calculated using the harmonic balance equations given in Johnson (1980). These equations were reasonably effective at generating a trimmed solutions for hover and forward flight conditions where stall effects were not significant. Where stall is significant, however, these control angles will usually need to be adjusted through some automatic control procedure in order to obtain an acceptably trimmed solution.

2.3 Piezoelectric control moment formulation

Bent, et al (1995), developed actuator equations for piezoelectric fiber composites using conventional poling. We will follow their approach here, although we will assume an interdigitated electrode scheme (Hagood, et al, 1993). Their notation has been adapted accordingly.

Assuming in-plane structural anisotropy in the piezoelectric material, and further assuming conditions of plane stress ($T_3=T_4=T_5=0$), the standard linear piezoelectric constitutive relations (ANSI/IEEE Std 176-1987, 1988) may be rewritten as

$$\begin{Bmatrix} D_1 \\ D_2 \\ D_3 \\ S_1 \\ S_2 \\ S_6 \end{Bmatrix} = \begin{bmatrix} \varepsilon_{11}^T & 0 & 0 & d_{11} & d_{12} & 0 \\ 0 & \varepsilon_{22}^T & 0 & 0 & 0 & d_{26} \\ 0 & 0 & \varepsilon_{33}^T & 0 & 0 & 0 \\ d_{11} & 0 & 0 & s_{11}^E & s_{12}^E & 0 \\ d_{12} & 0 & 0 & s_{12}^E & s_{22}^E & 0 \\ 0 & d_{26} & 0 & 0 & 0 & s_{66}^E \end{bmatrix} \begin{Bmatrix} E_1 \\ E_2 \\ E_3 \\ T_1 \\ T_2 \\ T_6 \end{Bmatrix} \tag{19}$$

or more compactly

$$\begin{Bmatrix} \mathbf{D} \\ \mathbf{S} \end{Bmatrix} = \begin{bmatrix} \boldsymbol{\varepsilon}^S & \mathbf{d} \\ \mathbf{d}^t & \mathbf{s}^E \end{bmatrix} \begin{Bmatrix} \mathbf{E} \\ \mathbf{T} \end{Bmatrix} \tag{20}$$

where

$$\mathbf{D} \equiv \begin{Bmatrix} D_1 \\ D_2 \\ D_3 \end{Bmatrix} \quad \mathbf{E} \equiv \begin{Bmatrix} E_1 \\ E_2 \\ E_3 \end{Bmatrix} \quad \mathbf{S} \equiv \begin{Bmatrix} S_1 \\ S_2 \\ S_6 \end{Bmatrix} \quad \mathbf{T} \equiv \begin{Bmatrix} T_1 \\ T_2 \\ T_6 \end{Bmatrix} \tag{21}$$

As in Bent, et al (1995), the S_3, S_4, and S_5 strains, although not necessarily zero, have been neglected here. Note that we have assumed poling of the piezoelectric material in the 1-direction, instead of the standard 3-direction, in accordance with the assumption of IDE poling.

Rewriting Eq. (20) with strains (**S**) as independent variables yields

$$\begin{Bmatrix}\mathbf{D}\\ \mathbf{T}\end{Bmatrix}=\begin{bmatrix}\varepsilon^S & \mathbf{e}\\ -\mathbf{e}^t & \mathbf{c}^E\end{bmatrix}\begin{Bmatrix}\mathbf{E}\\ \mathbf{S}\end{Bmatrix} \tag{22}$$

where

$$\mathbf{c}^E=\left(\mathbf{s}^E\right)^{-1}\quad \mathbf{e}=\mathbf{d}\mathbf{c}^E\quad \varepsilon^S=\varepsilon^T-\mathbf{d}\mathbf{c}^E(\mathbf{d})^t \tag{23}$$

The relationships between field components given in the global, or beam coordinate system, and those in a system rotated by an angle θ_{ply} about the 3-direction (see Fig. 3) are given by

$$\tilde{\mathbf{D}}=\mathbf{R}_E\mathbf{D}\quad \tilde{\mathbf{E}}=\mathbf{R}_E\mathbf{E}\quad \tilde{\mathbf{S}}=\mathbf{R}_S\mathbf{S}\quad \tilde{\mathbf{T}}=\left(\mathbf{R}_S{}^t\right)^{-1}\mathbf{T} \tag{24}$$

where $\mathbf{R_E}$ and $\mathbf{R_S}$ are respectively the applicable matrix of direction cosines and strain transformation matrix (see Jones (1975)). In terms of the actuator coordinate system, Eq. (22) then becomes

$$\begin{Bmatrix}\tilde{\mathbf{D}}\\ \tilde{\mathbf{T}}\end{Bmatrix}=\begin{bmatrix}\tilde{\varepsilon}^S & \tilde{\mathbf{e}}\\ -\tilde{\mathbf{e}}^t & \tilde{\mathbf{c}}^E\end{bmatrix}\begin{Bmatrix}\tilde{\mathbf{E}}\\ \tilde{\mathbf{S}}\end{Bmatrix} \tag{25}$$

Substituting Eq. (24) into Eq. (25) yields constitutive relations expressed in terms of the global field variables.

$$\begin{Bmatrix}\mathbf{D}\\ \mathbf{T}\end{Bmatrix}=\begin{bmatrix}\mathbf{R}_E{}^t\tilde{\varepsilon}^S\mathbf{R}_E & \mathbf{R}_E{}^t\tilde{\mathbf{e}}\mathbf{R}_S\\ -\mathbf{R}_S{}^t\tilde{\mathbf{e}}^t\mathbf{R}_E & \mathbf{R}_S{}^t\tilde{\mathbf{c}}^E\mathbf{R}_S\end{bmatrix}\begin{Bmatrix}\mathbf{E}\\ \mathbf{S}\end{Bmatrix} \tag{26}$$

For convenience, the electric fields and displacements will be defined as being specified along the actuator system 1-direction only. As a simplifying abstraction, the electric field within the piezoelectric material will also be assumed to be an average of the field strength between alternating electrodes. Equation (26) then reduces to

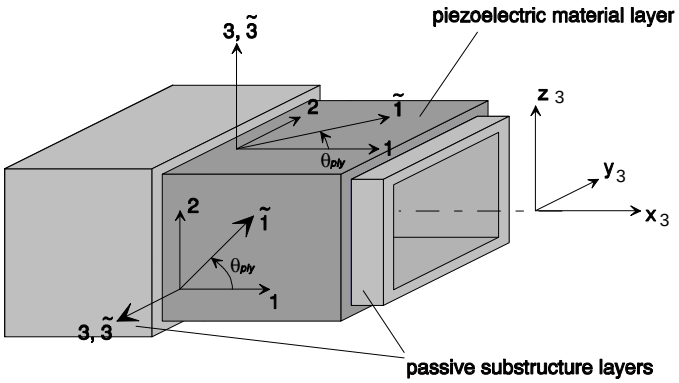

Figure 3. Material axes for piezoelectric layer. (Note that with an interdigitated electrode poling scheme, material is polarized along the $\tilde{1}$ direction.)

$$\begin{Bmatrix}\tilde{D}_1\\ \mathbf{T}\end{Bmatrix}=\begin{bmatrix}\tilde{\varepsilon}_{11}^S & \tilde{\mathbf{e}}\mathbf{R}_S\\ -\mathbf{R}_S{}^t\tilde{\mathbf{e}}^t & \mathbf{R}_S{}^t\tilde{\mathbf{c}}^E\mathbf{R}_S\end{bmatrix}\begin{Bmatrix}\tilde{E}_1\\ \mathbf{S}\end{Bmatrix} \tag{27}$$

From Eq. (27), we can extract the stresses in the piezoelectric material arising solely from the application of an electric field, i.e.,

$$\mathbf{T}_{PE}=-\mathbf{R}_S{}^t\tilde{\mathbf{e}}^t\tilde{E}_1 \tag{28}$$

A piezoelectric ply orientation angle which maximizes the actuator induced shear stress (T_6) is desired for the present study. This will occur for orientation angles of $\theta_{ply}=\pm 45°$. Equation (28) then, for the case of $\theta_{ply}=+45°$, may be expanded as

$$\mathbf{T}_{PE}=\begin{Bmatrix}T_{1PE}\\ T_{2PE}\\ T_{6PE}\end{Bmatrix}=\begin{Bmatrix}-\frac{1}{2}\left(\tilde{e}_{11}+\tilde{e}_{12}\right)\\ -\frac{1}{2}\left(\tilde{e}_{11}+\tilde{e}_{12}\right)\\ -\frac{1}{2}\left(\tilde{e}_{11}-\tilde{e}_{12}\right)\end{Bmatrix}\tilde{E}_1 \tag{29}$$

For the idealized closed, rectangular, thin-walled section considered here, the total piezoelectric induced bending moment may be found to be

$$M_{PE}=\oint z_3T_{1PE}t_{PE}ds \tag{30}$$

where t_{PE} is the total thickness of all piezoelectric laminae. If the applied electric field and piezoelectric laminate properties of the spar structure do not vary around the contour, we can see immediately that the piezoelectric bending moment will be identically zero.

The piezoelectric induced shear flow for this structure, q_{PE},, may be written as

$$q_{PE}=T_{6PE}t_{PE} \tag{31}$$

The total piezoelectric torsional moment is thus

$$\begin{aligned}Q_{PE}&=\oint rq_{PE}ds\\ &=2hwq_{PE}=-2A_e\tfrac{1}{2}\left(\tilde{e}_{11}-\tilde{e}_{12}\right)\tilde{E}_1t_{PE}\end{aligned} \tag{32}$$

where h and w are the height and width of the rectangular cross-section, and A_e is the area enclosed by the wall centerline.

Expressing Eq. (32) in terms of the free strain piezoelectric coefficients, yields

$$Q_{PE}=-A_e\left(d_{11}\left(\tilde{c}_{11}^E-\tilde{c}_{12}^E\right)+d_{12}\left(\tilde{c}_{12}^E-\tilde{c}_{22}^E\right)\right)\tilde{E}_1t_{PE} \tag{33}$$

Table 1. Lamina structural properties. (Piezoelectric lamina properties adapted from Rogers and Hagood (1995).)

Property	passive structure	IDE/MON	IDE/PFC	DAP/PFC
c_{11} , GPa	88	66	31	31
c_{22}/c_{11}	1	1	0.60	0.60
c_{12}/c_{11}	0.375	0.29	0.24	0.24
c_{66} , GPa	28	23	5.7	5.7
d_{31}/d_{33}	-	-0.5	-0.4	1
ρ, kg/m^3	280	750	580	580
Λ_{max}	-	500 με	500 με	250 με

For further convenience, we will rewrite Eq. (33) in terms of an assumed maximum produceable piezoelectric strain, Λ_{max}, , or

$$Q_{PE} = -A_e \tilde{c}_{11}^E \left[\left(1 - \frac{\tilde{c}_{12}^E}{\tilde{c}_{11}^E} \right) + \frac{d_{12}}{d_{11}} \left(\frac{\tilde{c}_{12}^E}{\tilde{c}_{11}^E} - \frac{\tilde{c}_{22}^E}{\tilde{c}_{11}^E} \right) \right] \Lambda_{\max} t_{PE} \frac{\tilde{E}_1}{\tilde{E}_{1\max}} \quad (34)$$

where $\Lambda_{\max} \equiv d_{11} \tilde{E}_{1\max}$. Material properties appearing in Eq. (34) for the piezoelectric laminae used in the numerical portion of this study are given in Table 1.

3. NUMERICAL IMPLEMENTATION

The equations of motion for the structural and aerodynamic degrees of freedom are rewritten in state variable form for numerical integration. For N radial aerodynamic points, the resulting state space model will consist of a system of *2(L+M)+5N* first order differential equations with, in general, time varying coefficients. These state variable equations are numerically integrated using a fourth and fifth order Runge-Kutta-Fehlberg algorithm, with the integrations performed with respect to rotor azimuth angle, ψ.

For the numerical case studies presented in this paper, we have used one out-of-plane bending mode and three torsional modes. Here, $W_1(\bar{x})$ was defined as the linear rigid body flapping deflection mode shape, and $\Phi_m(\bar{x})$ were assumed to be the first three torsional comparison functions developed by Karunamoorthy and Peters (1987). Use of polynomial approximations instead of the exact nonrotating mode shapes was done solely to simplify calculation of the integral coefficients appearing in Eq. (6) and Eq. (7).

4. RESULTS AND DISCUSSION

4.1 Piezoelectric twist actuated rotor blade conceptual design

Three conceptual piezoelectric induced twist rotor blade designs were examined in this study. These designs were developed in order to illustrate the twist actuation capabilities of the three general cases of piezoelectric actuation suggested by inspection of Eq. (34). These three general cases are:

Table 2. Baseline helicopter rotor parameters.

Parameter	Baseline value
Ω (rad/sec)	23.2
R (m)	8.54
γ	9.44
c/R	0.0488
Q	4
σ	0.0622
C_T	0.00465
$f/\pi R^2$	0.015
$\bar{\omega}_\theta = \sqrt{K_\theta / \Omega^2 I_\theta}$	16.0
I_θ/I_β	0.000327
e/c	0
$GJ/I_\beta \Omega^2 R$	0.00552
h (m)	46.7e-3
w (m)	155e-3
t (m)	3.58e-3
$\bar{\omega}_\beta$	1.0
$\bar{\omega}_{\phi_1}$	6.10
$\bar{\omega}_{\phi_2}$	18.19
$\bar{\omega}_{\phi_3}$	61.02

Case 1: $d_{12} \neq d_{11}$, $\tilde{c}_{11}^E = \tilde{c}_{22}^E$. This is the case of actuation lamina possessing piezoelectric free-strain anisotropy, and in-plane stiffness isotropy. This corresponds to a configuration where actuation layers are composed of solid, or monolithic, PZT materials, and are polarized according to the IDE scheme. This case will be referred to as IDE/MON for the remainder of the discussion.

Case 2: $d_{12} \neq d_{11}$, $\tilde{c}_{11}^E \neq \tilde{c}_{22}^E$. This is the case where the actuation lamina possess both free-strain and stiffness anisotropy. This would be true of a piezoelectric fiber composite, interdigitated electrode actuation scheme. This case will be referred to as IDE/PFC.

Case 3: $d_{12} = d_{11}$, $\tilde{c}_{11}^E \neq \tilde{c}_{22}^E$. This is the case of free-strain isotropy (or near isotropy) but with stiffness anisotropy in the actuating layers. This would be the case for a piezoelectric fiber composite structure utilizing a conventional poling scheme, or in an idealized sense, a case similar to the Directionally Attached Piezoelectric scheme originally proposed by Barret (1990). This scheme will be referred to as DAP/PFC in the following sections.

Stiffness, inertial, and actuation parameters for three conceptual helicopter blade designs, each representing one of the three cases above, were developed using full-scale helicopter parameters for a Sikorsky H-34 main rotor blade (Scheiman, 1964). The H-34 main rotor blade is a relatively simple, closed-section spar structure, and was easily idealized as a rectangular box section for the purposes of this study. These baseline blade parameters are summarized in Table 2. Structural parameters not identical to the baseline blade parameters are shown for each of the piezoelectric twist blade designs in Table 3.

Table 3. Structural parameters for numerical examples.

Parameter	IDE/MON	IDE/PFC	DAP/PFC
$GJ/I_\beta\Omega^2R$	0.00447	0.00365	0.00365
γ	8.28	8.28	8.28
t_{PE}/t	0.1875	0.300	0.300
$\overline{\omega}_\beta$	1.0	1.0	1.0
$\overline{\omega}_{\phi_1}$	5.60	5.14	5.14
$\overline{\omega}_{\phi_2}$	16.64	15.22	15.22
$\overline{\omega}_{\phi_3}$	59.67	58.58	58.58

Uniform blade properties were assumed in each case for simplicity. The piezoelectric material thickness fractions, t_{PE},, given here were calculated assuming that the blade total mass of each design could be no greater than 120% of the baseline full-scale helicopter blade mass. (The choice of 120% was essentially

Table 4 Aerodynamic parameters for numerical cases.

Parameter	Value
c_1	$-\frac{\pi}{4}\left(1+1.4M^2\right)$
c_2	c_1
c_3	$-\frac{3\pi}{16}\left(-1.26-1.53\tan^{-1}\left(15(M-0.7)\right)\right)$
M	0.30
$\overline{y}_{ac}$	0
N	5
$\overline{x}_i$	{0.28 0.44 0.60 0.76 0.92}
Δ_i	{0.16 0.16 0.16 0.16 0.16}

arbitrary, but represents a reasonable weight constraint on the design of the conceptual piezoelectric twist blades.) As a result, the torsional natural frequencies of the blade structures vary somewhat from the baseline design. Aerodynamic parameters used in the numerical case studies were not varied between the designs, and are shown in Table 4.

4.2 Numerical twist actuation authority results

Numerically generated twist actuation authority results for each of the three piezoelectric induced twist blade designs are shown in Figs. 2-4. These results are for a typical one-g hovering flight condition, which corresponds to a thrust coefficient of C_T = 0.00465. One electrode segment extending from $\overline{x} = 0,1$ is assumed for all three structures. A sinusoidal electric field input with linearly increasing frequency and peak amplitude of $E_{1\max}$ was used to generate the frequency responses (amplitude and phase with respect to the electric field input signal) shown in the figures. In these figures the elastic twist is defined as the difference between the elastic torsional deflection at the blade tip and that at the blade root.

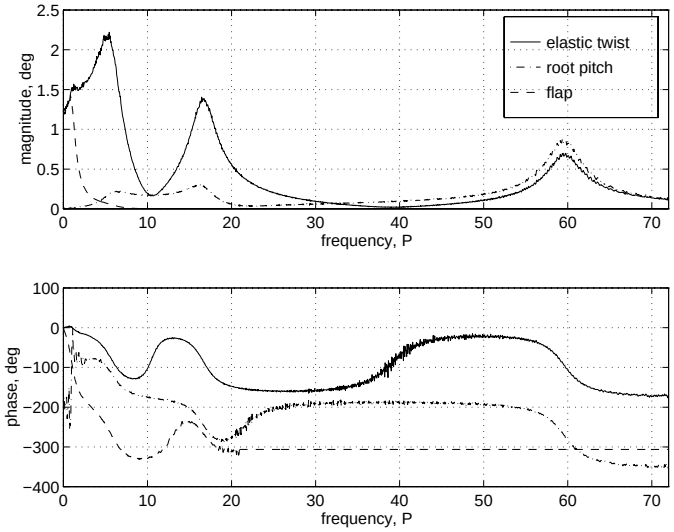

Figure 4. Blade frequency response: monolithic PZT twist actuation with interdigitated electrode poling scheme (IDE/MON); C_T = 0.00465, μ = 0.0.

Figure 4 illustrates the structural response of the IDE/MON case. A sustained oscillatory elastic twist magnitude of approximately ±1.25° to ±1.5° is generated for excitation frequencies below the first torsional frequency. At the first torsional resonance, which is predominately an elastic torsional response, the amplitude increases to approximately ±2.25°. A smaller torsional response occurs at the second and third torsional resonance frequencies.

The resonant response at the second and third torsional frequencies was found to vary widely depending on the amount of material and aerodynamic damping present in the structure. As the

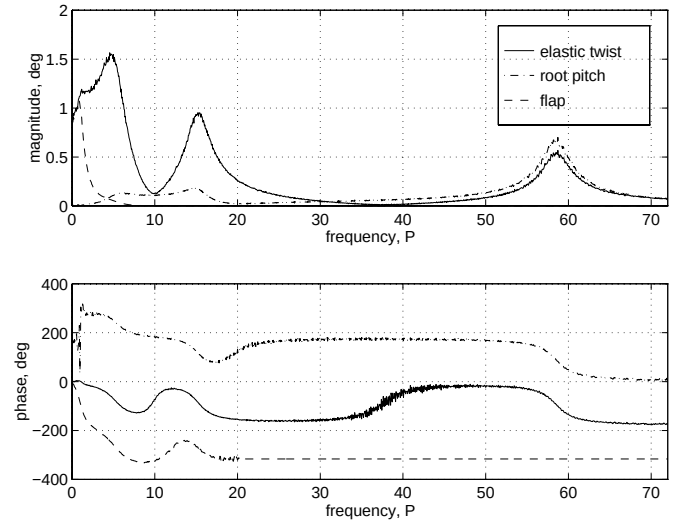

Figure 5. Blade frequency response: PFC twist actuation with interdigitated electrode poling scheme (IDE/PFC); C_T= 0.00465, μ = 0.0.

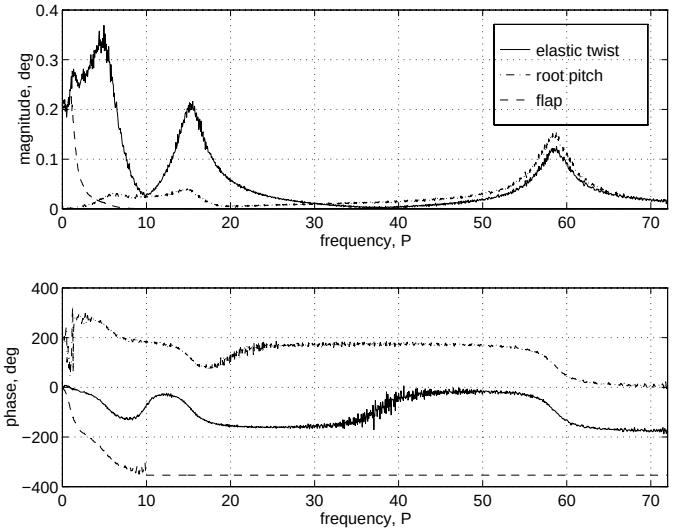

Figure 6. Blade frequency response: PFC twist actuation with conventional electrode poling scheme (DAP/PFC); C_T=0.00465, μ = 0.0.

torsional aerodynamic damping, from Eq. (18), is in general proportional to $\bar{b}^2$, the corresponding aerodynamic damping for these two modes is almost negligible. Some additional form of damping is desirable then at these higher frequencies to avoid unrealistically large torsional deflections. As such, a level of material damping equivalent to 0.5% of critical damping was assumed for each of the cases presented here.

The actuation results for the IDE/PFC lamina design are shown for the same flight condition in Fig. 5. A level of actuation capability on the order of ±1° to ±1.25° of elastic twist below the first torsional

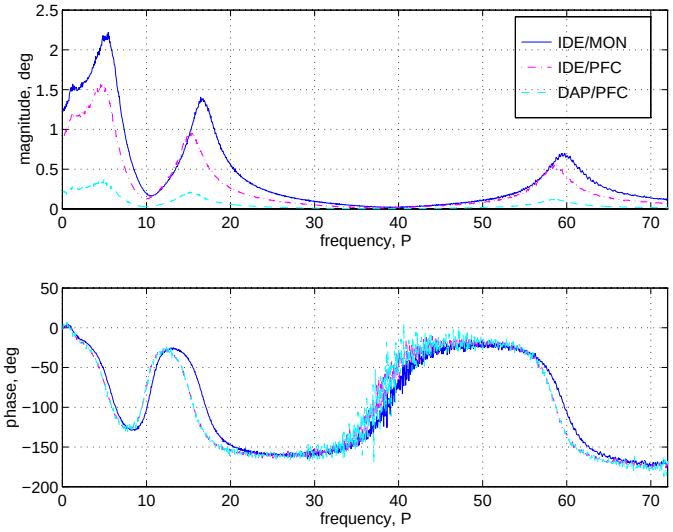

Figure 7. Comparison of elastic twist frequency response for IDE/MON, IDE/PFC, and DAP/PFC actuation schemes; C_T = 0.00465, μ = 0.0.

resonance, and ±1.5° at the first torsional mode resonance frequency is shown here. This is a level of performance slightly less than that demonstrated with the IDE/MON configuration. Although this may seem to imply that monolithic PZT laminae are more desirable for inclusion in piezoelectric actuated structures, manufacturing and poling nonplanar composite structures with solid PZT layers may not be practical. Piezoelectric fibers on the other hand could be incorporated into complex composite aerospace structures using, for the most part, established fiber composite construction techniques.

Figure 6 displays the twist actuation capabilities of the DAP/PFC blade design. Structurally, the DAP/PFC blade is identical to the IDE/PFC blade design, although the DAP/PFC blade utilizes conventional poling of the piezoelectric fibers. Relatively low nonresonant twist actuation is demonstrated for this actuation case, i.e., around ±0.2° to ±0.25° of elastic twist.

Comparison of the elastic twist actuation response of all three cases is shown in Fig. 7. The effect of the large free-strain anisotropies present in the IDE schemes on the magnitude of elastic twist is readily apparent. Both IDE poling cases exhibit generally four to five times the twist actuation magnitudes of the conventionally poled configuration. Such magnitudes of elastic twist are generally regarded as being sufficient for practical use in a vibration reduction scheme using individually controllable blade twist.

5. CONCLUSIONS

A simple helicopter rotor blade aeroelasticity analysis was developed and used to numerically demonstrate the twist actuation potential of embedded piezoelectric actuators for three nominally full-scale helicopter rotor blade designs. It was numerically demonstrated that useful nonresonant levels of oscillatory blade twist, i.e., on the order of ±1°, can potentially be produced without the addition of an excessive amount of piezoelectric actuator mass or saturation of the piezoelectric actuator materials, using an interdigitated electrode poling scheme with either a piezoelectric fiber composite or monolithic PZT actuation design.

The analysis and numerical model in its present form (i.e., with rigid flapping, elastic torsion and stall aerodynamics), should be sufficient for an examination of the potential of piezoelectric twist actuation to alleviate high oscillatory control loads induced by blade stall flutter (Ham and Young, 1966). Such a study is underway by the authors. Improvements to this model, such as the addition of multiple flapwise bending modes and a simple nonuniform inflow model, are also being undertaken.

REFERENCES

ANSI/IEEE Std 176-1987, IEEE Standard on Piezoelectricity, 1988.

Barrett, R., "Intelligent Rotor Blade Structures Development Using Directionally Attached Piezoelectric Crystals," M.S. thesis, University of Maryland, College Park, MD, 1990.

Bent, A., and Hagood, N., "Improved Performance in Piezoelectric Fiber Composites Using Interdigitated Electrodes," *SPIE Smart Structures and Materials 1995, Feb. 27-28 1995, Smart Materials, Proceedings*, Vol. 2441, 1995, pp. 196-212.

Bent, A., Hagood, N., and Rodgers, J., "Anisotropic Actuation with Piezoelectric Fiber Composites," *Journal of Intelligent Material Systems and Structures*, Vol. 6, May 1995, pp. 338-349.

Chen, P., and Chopra, I., “A Feasibility Study to Build a Smart Rotor: Induced Strain Actuation of Airfoil Twisting Using Piezoceramic Crystals,” *SPIE Smart Structures and Materials Conference, Feb. 1-4 1993, Smart Structures and Intelligent Systems, Proceedings*, Vol. 1917, Part 1, 1993, pp. 238-254.

Derham, R., and Hagood, N., "Rotor Design Using Smart Materials to Actively Twist Blades," *American Helicopter Society 52nd Annual Forum Proceedings*, Vol. 2, Washington, D.C., June 4-6, 1995, pp. 1242-1252.

Duncan, W., "Galerkin's Method in Mechanics and Differential Equations," Aeronautical Research Council Report and Memo 1798, August 1937.

Gessow, A., and Meyers, G., C., Jr., *Aerodynamics of the Helicopter*, College Park Press, 1952.

Giurgiutiu, V., Chaudhry, Z., Rogers, C., "Engineering Feasibility of Induced Strain Actuators for Rotor Blade Active Vibration Control," *Journal of Intelligent Material Systems and Structures*, Vol. 6, No. 5, pp. 583-597, September 1995.

Hagood, N., Kindel, R., Ghandi, K., and Gaudenzi, P., "Improving Transverse Actuation of Piezoceramics Using Interdigitated Surface Electrodes," *SPIE Smart Structures and Materials Conference, Feb. 1-4 1993, Smart Structures and Intelligent Systems, Proceedings*, Vol. 1917, Part 1, 1993, pp. 341-352.

Ham, N., "Helicopter Individual-Blade-Control Research at MIT 1977-1985," *Vertica*, Vol. 11, 1987, pp. 109-122.

Ham, N., Young, M., "Torsional Oscillations of Helicopter Blades Due to Stall," *Journal of Aircraft*, Vol. 3, No. 3, pp. 218-224, May-June 1966.

Johnson, W., *Helicopter Theory*, Princeton University Press, 1980.

Jones, R. M., *Mechanics of Composite Materials*, McGraw-Hill, 1975.

Karunamoorthy, S., Peters, D., "Use of Heirarchical Elastic Blade Equations and Automatic Trim for Rotor Response," *Vertica*, Vol. 11, No. 1/2, 1987, pp. 233-248.

Kaza, K. R. V., and Kvaternik, R. G., "Nonlinear Aeroelastic Equations for Combined Flapwise Bending, Chordwise Bending, Torsion, and Extension of Twisted Nonuniform Rotor Blades in Forward Flight," NASA TM 74059, August 1977.

Loewy, R., "Helicopter Vibrations: A Technological Perspective," *Journal of the American Helicopter Society*, Vol. 29, No. 4, October 1984, pp. 4-30.

Nitzsche, F., Breitbach, E., "Using Adaptive Structures to Attenuate Rotary Wing Aeroelastic Response," *Journal of Aircraft*, Vol. 31, No. 5, 1994, pp. 1178-1188.

Peters, D. A., “Toward a Unified Lift Model for Use in Rotor Blade Stability Analyses,” *Journal of the American Helicopter Society*, Vol. 30, No. 3, pp. 32-42, July, 1985.

Peters, D. A., Chouchane, M., and Fulton, M., “Helicopter Trim with Flap-Lag-Torsion and Stall by an Optimized Controller,” *Journal of Guidance, Control and Dynamics*, Vol. 13, No. 5, pp. 824-834, Sept.-Oct., 1990.

Petot, D., "Differential Equation Modelling of Dynamic Stall," *Recherche Aerospatiale*, Vol. 5, No. 5, 1989.

Rehfield, L. W., "Design Analysis Methodology for Composite Rotor Blades," Seventh DoD/NASA Conference on Fibrous Composites in Structural Design, Denver CO, June 1985.

Reichart, G., "Helicopter Vibration Control - A Survey," Vertica, Vol. 5, No. 1, 1981, pp. 1-20.

Rodgers, J., Hagood, N., "Manufacture of Adaptive Composite Plates Incorporating Piezoelectric Fiber Composite Plies," *36th AIAA/ASME/ASCE/AHS/ASC Structures, Structural Dynamics, and Materials Conference and AIAA/ASME Adaptive Structures Forum, Technical Papers, Part 5*, New Orleans, LA, April 10-13, 1995.

Samak, D., Chopra, I., “A Feasibility Study to Build a Smart Rotor: Trailing Edge Flap Actuation,” *SPIE Smart Structures and Materials Conference, Feb. 1-4 1993, Smart Structures and Intelligent Systems, Proceedings*, Vol. 1917, Part 1, 1993, pp. 225-237.

Scheiman, J., "A Tabulation of Helicopter Rotor-Blade Differential Pressures, Stresses, and Motions as Measured in Flight," NASA TM X-952, March 1964.

Song, O., Librescu, L., “Vibrational Behavior of Rotating Helicopter Blades Incorporating Adaptive Capabilities,” *SPIE Smart Structures and Materials Conference, Feb. 1-4 1993, Smart Structures and Intelligent Systems, Proceedings*, Vol. 1917, Part 1, 1993, pp. 354-367.

Spangler, R. L., Jr. and Hall, S. R., "Piezoelectric Actuators for Helicopter Rotor Control,” *AIAA/ASME/ASCE/AHS/ASC 31st Structural Dynamics and Materials Conference, Apr. 2-4, 1990, Technical Papers*, AIAA Paper No. 90-1076, 1990, pp. 1589-1599.

Tang, D., private communication to W. K. Wilkie, August 1995.

Tran, C. T., and Petot, D., “Semi-Empirical Model for the Dynamic Stall of Airfoils in View of the Application to the Calculation of Responses of a Helicopter Blade in Forward Flight,” *Vertica*, Vol. 5, No. 1, pp. 35-53, 1981.

Wilkie, W. K., and Park, K. C., "An Aeroelastic Analysis of Helicopter Rotor Blades Incorporating Piezoelectric Fiber Composite Twist Actuation," NASA TM-110252, ARL-MR-328, May, 1996.